A Robotic Near-Field Antenna Test System Relying on Non-Canonical Transformation Techniques

Daniël Janse van Rensburg, Brett Walkenhorst, Quang Ton & John Demas
1125 Satellite Blvd., Suite 100, Suwanee, GA 30024-4629 USA

drensburg@nsi-mi.com
bwalkenhorst@nsi-mi.com
qton@nsi-mi.com
jdemas@nsi-mi.com

***Abstract* – A robotic near-field antenna measurement system allowing for acquisition over non-canonical measurement surfaces is presented. The robot consists of a six-axis robotic arm and a seventh axis rotary positioner and the created acquisition surface is parametrically reconfigurable. The near-field to far-field transformation required is also described. The success of the technique is demonstrated through measured results, compared to canonical measurement data.**

Keywords - Non-Canonical Near-Field, Antenna Measurements, Robotic.

I. Introduction

Robotic near-field antenna measurement systems have been presented in recent years [1] & [2] as alternatives to conventional near-field antenna test systems. The attraction of these systems is the perceived benefit of software reconfigurability. However, in all cases presented to date, these robotic test systems have attempted to replace existing (canonical) planar, cylindrical or spherical test systems. With the advent of near-field to far-field transformation techniques that do not rely on canonical planar, cylindrical or spherical wave expansions [3], the possibility of making near-field measurements on arbitrary surfaces has become a reality. Robotic positioners provide the ideal tool for such implementations, and in this paper, we describe such a near-field antenna test system.

We describe this test system in detail in Section 2. The near-field to far-field transformation methodology employed here requires an equivalent current surface [3] to be defined and we describe the technique in broad terms in Section 3. In Section 4 we present initial test data obtained and we compare those results to data obtained using a modal expansion technique. We present final conclusions in Section 5.

II. The Robotic Test System

The system we describe consists of a six-axis robotic arm and rotary positioner that allows for near-field acquisition over a parametrically reconfigurable measurement surface. This adjustability overcomes the limitations of traditional near-field test systems that are restricted to test surfaces that are planar, cylindrical, or spherical. One can thereby create a test system that is not only more space efficient, but also adaptable to many different types of antennas, thereby optimizing space usage.

The hardware is depicted in Figure 1 and it shows the single-axis rotator and the six-axis robotic arm. In this case, the antenna under test (AUT) is a slotted waveguide array and is mounted on the rotator, facing skywards. The six-axis robot describes a generatrix and the combined motion of the robot, and the rotator describes a surface of revolution.

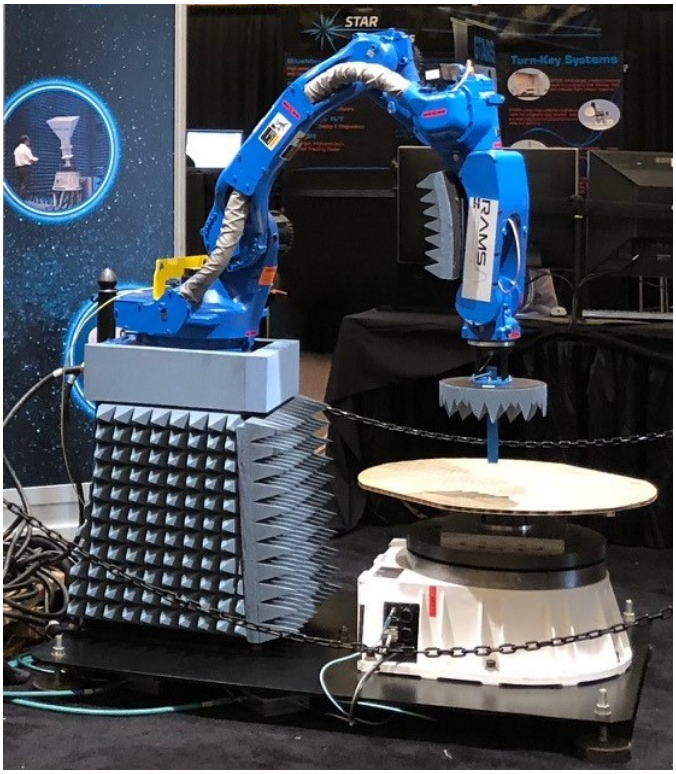

Figure 1: The six-axis robotic arm, rotation stage and AUT are shown. In this instance the AUT is a slotted waveguide array and the near-field probe is a linearly polarized open-ended waveguide probe.

The transformation software (described below in Section III) relies on sampled electromagnetic field values acquired at known positions (near-field probe orientation also needs to be known) on a surface close to the antenna under test. This surface does not have to be closed and the choice of test

surface can be made based on the characteristics of the antenna under test and the field of view required.

In this implementation, the test surface is a surface of revolution generated by defining a generatrix (half of the surface cross section) that is rotated around the axis of rotation. This rotational symmetry is our choice of implementation andis not required by the near-field to far-field transformation methodology employed here. The generatrix is depicted in Figure 2. Examples of such surfaces of revolution would be a circular plane (e.g. plane polar acquisition), a capped cylinder, a sphere, and an oblate spheroid. The test surface is created by moving a near-field probe along the generatrix and rotating the antenna under test. The generatrix is defined in the x/z plane, and in this implementation the robotic arm is used to trace the generatrix while the single-axis rotator is used to flesh out the full 3D surface.

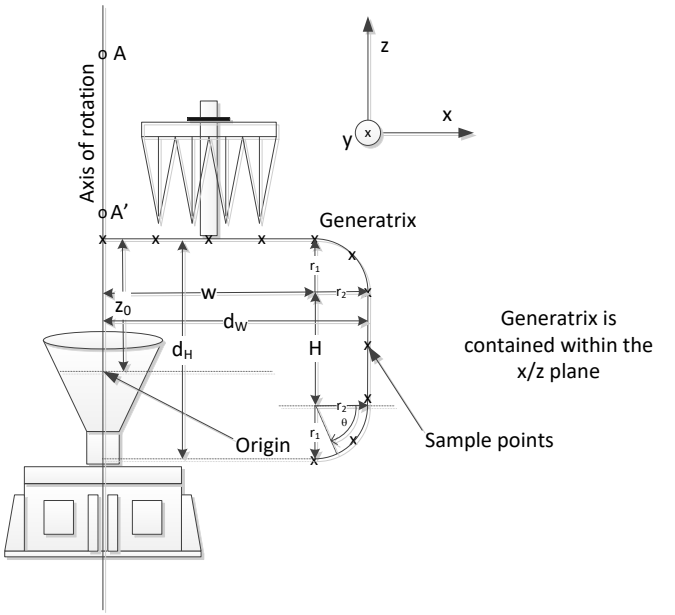

Figure 2: The generatrix parameters and coordinate system defined.

Figure 2 depicts the generatrix and its associated parameters. Electric field sample locations are indicated, and the distribution of these discrete locations are based on the electrical size of the AUT. The software allows the user to define and customize the specific surface. Motion of the near-field probe along the generatrix is such that the aperture of the probe remains tangential to the surface of revolution during acquisition. Motion along the generatrix is performed in discrete steps during acquisition (stop motion) while the rotation stage is kept moving continuously. Two orthogonal linear polarization components are measured during acquisition, one circumferentially directed (aligned with the y-axis in Figure 2) and a second that is tangential to the generatrix (parallel to the x/z plane in Figure 2).

The generatrix is defined by the following parameters:

d_W: The total radius of the test surface.
d_H: The total height of the test surface.
r_1: The starting radius of curvature of the corner of the test surface.
r_2: The ending radius of curvature of the corner of the test surface.
H: The vertical straight section of the test surface.
W: The horizontal straight section of the test surface.
θ: The angular extent of the lower curved corner of the test surface ($0° \leq \theta \leq 90°$).
z_0: The height of the test surface above the coordinate system origin.

These parameters simplify definition of the test surface and allow one to adapt the surface to many different types of antennas and allow for definition of the example scanning surfaces as shown in Table 1. The table shows typical values that allow the user to define:

- A plane polar scanning surface of diameter 2W.
- A capped cylindrical surface of diameter 2W.
- A hemi-spherical surface of radius $r_1 = r_2$.
- A partial oblate spheroid r_1 = minor axis and r_2 = major axis.
- A partial prolate spheroid r_1 = major axis and r_2 = minor axis.

Table 1: Examples values for the generatrix parameters and the surfaces that can be defined.

Scanning surface	d_W *[m]*	*W [m]*	d_H *[m]*	*H [m]*	r_1 *[m]*	r_2 *[m]*	*θ*	z_0 *[m]*
1m Radius plane-polar surface	1	1	0	0	0	0	0°	Arbitrary
0.5m Radius, 1m tall capped cylindrical surface	0.5	0.5	1	1	0	0	0°	1
0.5m Radius hemi-spherical surface	0.5	0	0.5	0	0.5	0.5	0°	0.5
0.5m Radius partial spherical surface	0.5	0	0.75	0	0.5	0.5	45°	0.75
Partial oblate spheroid	0.5	0	0.175	0	0.25	0.5	45°	0.175
Partial prolate spheroid	0.25	0	0.75	0	0.5	0.25	45°	0.75

Although the transform described in Section III allows for arbitrary test surfaces, the rotationally symmetric parametric surface defined here strikes a good balance between being highly customizable and presenting the user with a surface definition that is well characterized and therefore reduces risk of damage to the antenna under test.

For the AUT of 80 cm diameter presented here, a plane-polar scanning surface of 1 m diameter will support a ± 45°

far-field viewing angle (assuming a 3λ probe distance at X-band frequency). If we wanted to increase this to a ± 85° viewing angle, one would need a plane-polar scanning surface of 3 m diameter and larger viewing angles would not be possible to achieve.

If one considers a non-canonical acquisition surface, these angular limitations can be overcome as follows: If the robotic arm not only moves the probe along a straight line trajectory, but also turns the probe by 90° and we describe a capped cylinder (labelled below as a "pillbox" surface of test), one can achieve a ± 135° viewing angle for a cylinder diameter of 1 m and height of only 20 cm. This makes for a highly space-efficient test system. Since plane wave expansion is now not an option anymore, we must consider a specialized processing technique (described in Section III) implemented as a software tool we refer to as FlexForm.

We can also consider a traditional Spherical Near-Field (SNF) test system to overcome the angular limitations of the plane-polar technique. A typical test system would use a rigid swing-arm, attached to a rotary stage to describe a circular arc of the near-field probe (acting as θ positioner) while a second rotary positioner is used as ϕ positioner, rotating the AUT. An example of a such a test system is shown in Figure 3 below. It should be noted that this type of SNF test system is limited in that the probe radial distance is fixed and driven by the largest AUT to be tested. It therefore typically needs to be decided upon initial design of the test facility and gives the user limited flexibility when considering future upgrade options.

In what follows, we emulate this type of SNF acquisition using the robotic system and we use the data obtained in this way as reference against which we compare our non-canonical surface acquired and FlexForm processed data. In this instance the robotic arm describes a circular arc (effectively acting as θ positioner) while the rotary positioner will generate the spherical surface (effectively acting as ϕ positioner). Our NF to FF transformation will then rely on a standard Spherical Wave Expansion (SWE) technique [4]. In this instance the success of the method will hinge on the ability of the test hardware to create a perfect spherical surface with high fidelity. In the data comparison presented below, SNF data acquired in this fashion are compared to FlexForm results to illustrate the success of the non-canonical technique.

III. The Near-field to far-field transformation methodology

The non-canonical near-field to far-field transformation technique presented here addresses the need to perform near-field antenna measurements with improved flexibility as compared to the traditional approaches of canonical measurement surfaces using regular sampling. Inspired by the powerful fast integral equation solvers from computational electromagnetics, the approach relies on inverse equivalent source solvers for the transformation of measured near-field data into a set of equivalent sources. These sources, acting as proxies to the original AUT, can then be used to calculate near and far-fields. This enables near-field antenna measurements to be made on non-canonical surfaces and /or with irregular sampling grids. A by-product of these inverse equivalent sources solvers is that they allow a very flexible modeling of the antenna under test (AUT), which can, with the inclusion of a priori knowledge about the geometric extent of the AUT, provide "measured" currents on the antenna structure [4].

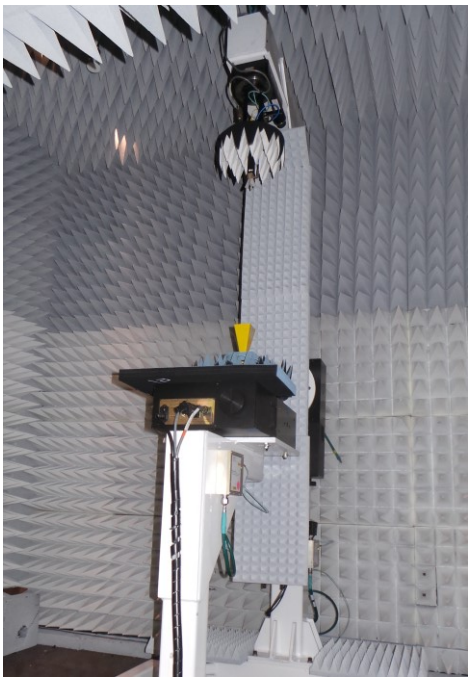

Figure 3: A swing arm (θ/ϕ) spherical near-field antenna test system used for mm-wave applications.

The canonical field transformations used in industry are based on an expansion of the antenna radiation fields into modal solutions of Maxwell's equations. Such field modes represent a complete set of vector expansion functions for the radiation fields. Each of these individual modes are mutually orthogonal when evaluated on the corresponding coordinate surfaces, e.g., on planes, cylinders, or spheres. Based on regular equidistant sampling of the measured fields on these surfaces, and by utilizing Fast Fourier Transform (FFT) based algorithms, it is possible to realize efficient and very robust antenna field transformations. Due to the availability of these methods, it is common in the antenna measurement community to adapt the measurement hardware and configurations to the needs of the available field transformation approaches.

Although the theory supports field transformations for irregularly spaced measurement samples on non-canonical surfaces, the available algorithms and the available computers were previously not powerful enough to render such field transformations practical. The growth of computing resources in recent years and the availability of robotic hardware now allow us to use these fast integral equation solvers in the way described here.

An additional aspect of this approach is that these algorithms not only support irregular sampling on arbitrary measurement surfaces, but they are commonly also based on very flexible radiation models of the AUT. Since the AUT radiation is represented by equivalent sources, which exist on a

surface enclosing the actual AUT, knowledge about the size and shape of the AUT can be considered in setting up the equivalent radiation model. These equivalent sources are based on the well-known surface equivalence theorem in electromagnetics [5].

The measurement sequence in this case requires a near-field measurement to be performed by moving a near-field probe over a surface described by the generatrix shown in Figure 2. Through combined motion of the robotic arm and the rotary positioner, electric field values are acquired at discrete coordinates and can be denoted as $\boldsymbol{E}(x_i, z_i, \phi_i)$. A distribution of these sample points for the example of interest here is as depicted in Figure 4. In this image, each blue dot represents a grid point on the non-canonical measurement surface where two orthogonal electric field samples are acquired.

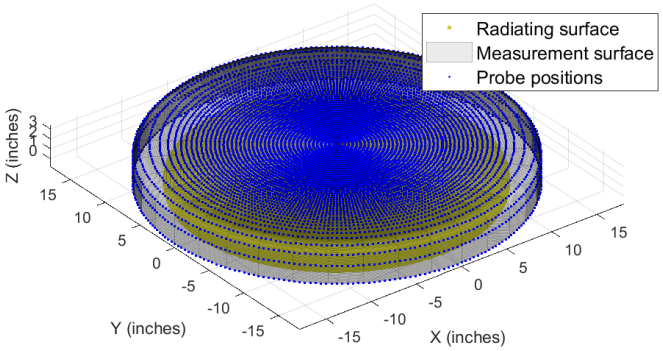

Figure 4: Graphical representation of the field sample locations (blue dots) where near-field samples are acquired on the capped cylinder.

The magnitude of the acquired electric field values is shown as a false color image in Figure 5 and the shape of the capped cylindrical surface is clear.

Following this acquisition, the user has to select a surface enclosing the AUT. We will call this the *AUT Bounding Surface* in contrast to the *Measurement Surface*. This surface is where the equivalent sources are to be computed and from which all final near-field and far-field values are derived. Since this is a process based on computational electromagnetics principles, this surface has to be discretized and aspects like solution convergence need to be considered. An example AUT bounding surface, discretized, is depicted in Figure 6.The AUT bounding surface for the slotted waveguide depicted in Figure 1 is cylindrical and of an electrical size that makes its discretization difficult to discern. We therefore show a much smaller, discretized surface to illustrate the concept. The user has significant freedom in the selection of this surface. In general, it does not need to conform to the AUT surface, but it must enclose all parts of the AUT, and it cannot extend beyond the measurement surface. It also needs to be separated from the measurement surface by more than a few wavelengths to ensure that reactive coupling between the measured field samples and the equivalent currents can be neglected. Finally, selection of the equivalent surface to be conformal to the AUT surface can be very advantageous for diagnostics purposes, but alignment of this surface with respect to the actual AUT needs to be carefully planned and executed.

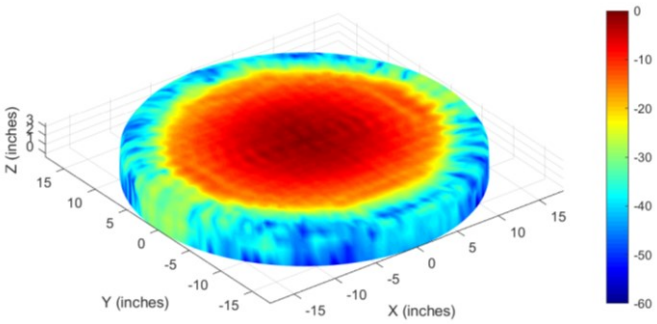

Figure 5: Graphical representation of the electric field amplitude of the field samples acquired.

Once the equivalent source currents have been resolved, we have a representation of the AUT that enables one to compute all radiation parameters of interest, exterior to the AUT bounding surface. The computational effort to obtain these surface currents is estimated to be roughly an order of magnitude more demanding than that for traditional modal techniques. However, this comes with the added advantage of a test solution than can be tailored for the specific AUT (making for a more space efficient solution) and it allows one to circumvent the need for precise mechanical near-field probe positioning in exchange for knowing the precise near-field probe location.

IV. Measured Results

As validation of this test system, a known AUT was selected and tested using a traditional SWE near-field technique and subsequently using the FlexForm technique. The AUT was a 30" diameter slotted waveguide array as depicted in Figure 1. For the spherical acquisition, the robotic arm was used as θ-axis and the rotary positioner was used as ϕ-axis. Near-field to far-field processing was performed using a regular modal expansion technique, and the principal plane radiation patterns are depicted by the dashed lines in Figure 7.

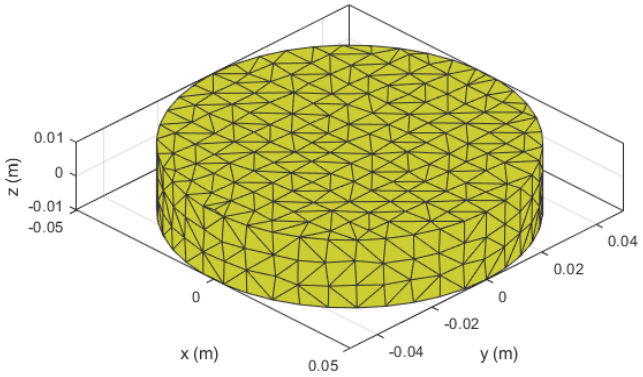

Figure 6: Example discretized AUT bounding surface.

We subsequently also measured the AUT using a capped cylinder measurement surface, sampling on a grid of points as depicted in Figure 4. We then defined a thin cylindrical AUT

bounding surface, solved for the equivalent surface currents, and based on these, computed the far-field radiation patterns. These radiation patterns are depicted by the solid lines in Figure 7 and overlaid on the modal based results.

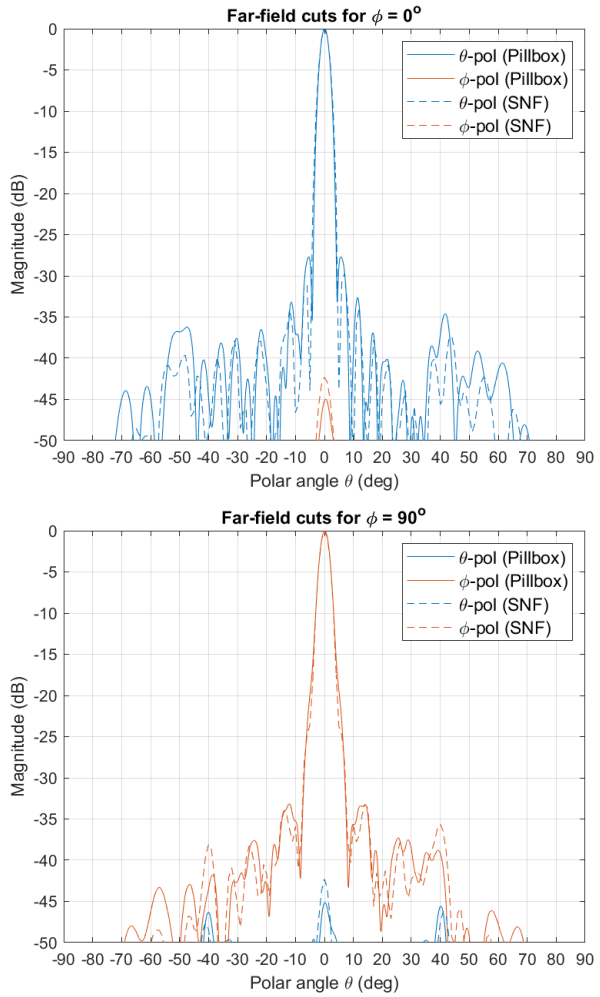

Figure 7: Orthogonal principal plane radiation pattern cuts shown for the AUT. FlexForm result is depicted as the solid lines and Spherical Near-Field as dashed lines.

The radiation pattern comparisons in Figure 7 display a level of disagreement that can be improved upon. This can be ascribed to the fact that these measurements were conducted in a non-absorbered environment and the robotic arm also lacked absorber. This fact will lead to variations such as those observed here. However, further refinement of the testing is planned.

V. Conclusions

This paper presents a robotic near-field antenna measurement system that allows for acquisition on a non-canonical measurement surface. The software offered with this test system also allows for transformation of this near-field test data to a set of equivalent currents that represent the AUT. These currents (if the equivalent surface is selected appropriately) allow for AUT diagnostics and calculation of all radiated fields. The software associated with this transformation process is called FlexForm. This test system offers the user a degree of flexibility that is not possible with conventional (canonical) near-field antenna test systems. We present test data here that validates this approach by comparing test results obtained using a conventional spherical near-field technique to results obtained using the FlexForm system.

This test approach has the advantage of offering a solution that can be tailored for specific AUTs, optimizing space usage and reducing test time.

A final advantage of the FlexForm transformation is the ability to process near-field data based on knowledge of the actual location of data samples, instead of trying to position a near-field probe at a specific pre-defined location. This aspect can significantly change the design philosophy of high frequency near-field test systems.

References

[1] D. Novotny, J. Gordon, J. Coder, M. Francis & J. Guerrieri, "Performance evaluation of a robotically controlled millimeter-wave near-field pattern range at the NIST," Antennas and Propagation (EuCAP), 7th European Conference on Antennas and Propagation, pp.4086 -4089, 8-12 April 2013.

[2] J. Hatzis, P. Pelland & G. Hindman, "Implementation of a combination planar and spherical near-field antenna measurement system using an industrial 6-axis robot", AMTA 38th Annual Meeting & Symposium, Austin, Tx, Oct 2016.

[3] C. H. Schmidt, M. M. Leibfritz & T. F. Eibert, "Fully Probe-corrected near-field far-field transformation employing plane wave expansion and diagonal translation operators," IEEE Transactions on Antennas and Propagation, vol. 56, pp. 737-746, Mar 2008.

[4] C. Parini, S. Gregson, J. McCormick, D. Janse van Rensburg & T. Eibert, *Theory and Practice of Modern Antenna Range Measurements,* London, UK: The Institute of Engineering and Technology, 2019.

[5] R.F.Harrington, *Time-Harmonic Electromagnetic Fields,* McGraw-Hill, 1961.